Scaling behavior of disordered lattice fermions in two dimensions

Antonio Hill and Klaus Ziegler[a]

Institut für Physik, Universität Augsburg, 86135 Augsburg, Germany

Abstract. We propose a lattice model for Dirac fermions which allows us to break the degeneracy of the node structure. In the presence of a random gap we analyze the scaling behavior of the localization length as a function of the system width within a numerical transfer-matrix approach. Depending on the strength of the randomness, there are different scaling regimes for weak, intermediate and strong disorder. These regimes are separated by transitions that are characterized by one-parameter scaling.

1 Introduction

Two-dimensional (2D) Dirac fermions play a crucial role as quasiparticles in graphene and on the surface of topological insulators. A fascinating consequence of their appearance in graphene are the robust electronic transport and the optical properties in the vicinity of the two Dirac nodes, where two electronic bands meet each other with linear dispersion [1,2]. The appearance of the Dirac nodes is caused by the honeycomb lattice in graphene, which decomposes into two triangular sublattices. A similar band structure was discussed for a number of semiconductors [3]. This indicates that 2D Dirac fermions may play a crucial role in designing new materials with specific opto-electronic properties.

In contrast to the experimentally observed robust transport properties it has been claimed from the theoretical side that transport is very sensitive to whether inter-node scattering is present or not in the presence of disorder [4]. In particular, there have been speculations that electronic states are delocalized in the absence of inter-node scattering but localized in its presence. Several authors claimed that this can be explained by changing the symmetry class of the underlying Hamiltonian from symplectic to orthogonal [5,6]. These claims are based on weak-localization calculations [4,6], which predict weak (anti-)localization (with) without inter-node scattering. Since weak localization calculations can only indicate the tendency towards localization, it would be interesting to evaluate this effect directly in terms of the scaling behavior of the localization length. A step in this direction is a computer simulation of the conductivity, using the Landauer-Büttiker formalism, that shows that fermions on the honeycomb lattice undergo a metal-insulator transition for long-range random scalar potential with strong disorder [7].

We shall study in the following the localization length of a strip of finite width M under a change of M in this paper. Our method, originally introduced for transfer-matrix calculations of the Schrödinger Hamiltonian [8–10], will be applied subsequently to 2D lattice Dirac fermions with one or more nodes. The same method has also been used to study the scaling behavior of network models (cf. [11,12]) or the brickwork lattice within the tight-binding formalism [13,14]. For this purpose we introduce a model which has two bands and four Dirac nodes. We can open a gap at one node and gaps for the other three nods independently. This allows us to study the effect of intervalley scattering by either keeping all four nodes or removing three of them and keeping only a single node.

The aim of this work is to understand the scaling behavior of the localization length in two dimensions in the metallic regime and near a metal-insulator transition due to a gap opening. The latter has been observed recently in graphene [15–17] where it appears in the presence of a random gap in the Dirac spectrum. If the average gap value is small in comparison to the fluctuation strength the system is metallic whereas it is insulating when the gap fluctuations are too weak in comparison to the average gap [18–20].

2 Model

A tight-binding description of electrons in graphene yields the famous energy dispersion with two separate nodes (or neutrality points) in the Brillouin zone. In the vicinity of these nodes the momentum dependence of the spectrum is found to be linear and the low-energy behavior of quasi particles can well be described by the Dirac equation $H\psi(x,y) = E\psi(x,y)$ with the Hamiltonian

$$H = -i\hbar v_F \left(\vec{\sigma} \cdot \vec{\nabla} \right) + v_F^2 m\sigma_3, \qquad (1)$$
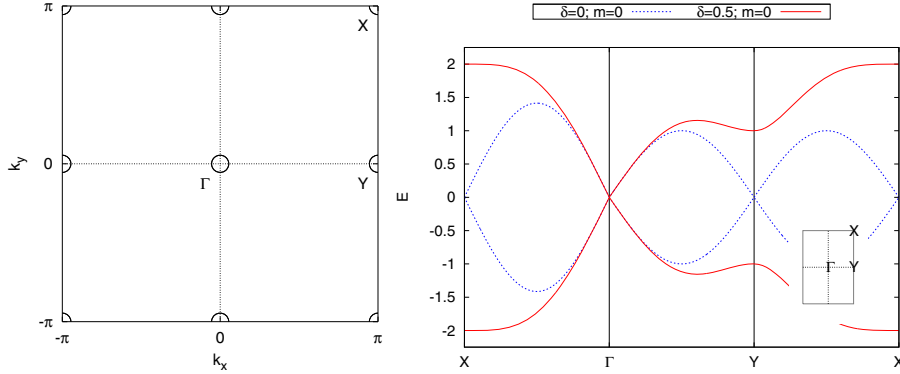
Fig. 1. Brillouin zone of the discrete Dirac equation with circles depicting the positions of the Dirac cones (left). A cut through the energy dispersion (8) in the two-dimensional k space with the points X, Y and Γ, as indicated in the inset, is shown on the right for $\delta = 0$ (blue line), $\delta = 0.5$ (red line).

where v_F is the Fermi velocity, $\vec{\sigma}$ is the vector of Pauli matrices and $\psi = (\varphi_1, \varphi_2)$ is the two component spinor wave function, furthermore, we set $\hbar v_F = 1$. The gap m can be of different origin: in graphene for example, a gap can be opened by breaking the sublattice symmetry, i.e. a staggered potential or by adsorption of atoms [16]. In a topological insulator the Dirac surface mode can be gapped due to local spins originating from magnetic dopants on the surface. Then, the mean density of local spins determines the gap width [21].

A numerical treatment of the Dirac equation requires a discretization in space. However, the naive discretization through replacing the differential operator by a difference operator leads to additional new nodes, which is often called fermion doubling or multiplication [22]. In real space there are two methods to circumvent this problem [5,23,24]. One that we will describe in this section goes back to the idea of Susskind. We start with discretizing the differential operator in a symmetric way

$$\partial_x f(x) \approx \frac{1}{2\Delta}(f_{l+\Delta} - f_{l-\Delta}), \tag{2}$$

where Δ is the lattice constant which we set to unity in the following. The discrete Dirac equation for $m = 0$ then takes the form

$$-\frac{i}{2}\sigma_1 \{\psi_{l+1,n} - \psi_{l-1,n}\} - \frac{i}{2}\sigma_2 \{\psi_{l,n+1} - \psi_{l,n-1}\} = E\sigma_0 \psi_{l,n} \tag{3}$$

with lattice points given by the coordinates (l, n) with integer l and n. This lattice Hamiltonian can be understood as a tight-binding model for electrons on a lattice with sublattice structure. A well-known example is graphene. Off-diagonal elements of the Pauli matrices describe hopping between different sublattices. Fourier transformation provides the dispersion $E = \pm\sqrt{\sin(k_x)^2 + \sin(k_y)^2}$ which has four Dirac cones in the Brillouin zone corresponding to four Dirac fermions. In order to open a gap at three of them we introduce a lattice operator [25] which acts on a wave function as:

$$\hat{B}\psi_{l,n} = \frac{1}{2}\sigma_3 \{\psi_{l+1,n} + \psi_{l-1,n} + \psi_{l,n+1} + \psi_{l,n-1} - 4\psi_{l,n}\}. \tag{4}$$

Such a lattice term can appear, for instance, in the tight-binding representation on a surface of a topological insulator. It describes a nearest-neighbor hopping term on the same sublattice. As such it breaks the sublattice symmetry of the Hamiltonian in equation (3) with the effect that a gap opens. This leads to a discretized version of the Hamiltonian (1), where we include the lattice operator $\hat{B}$ and a random gap term

$$H \rightarrow H + \delta\hat{B} + m_{l,n}\,\sigma_3. \tag{5}$$

The parameter δ allows us to tune the contribution of the hopping on the same sublattice. Then the Hamiltonian can also be written as:

$$H_{r'r} = \varepsilon_r\,\delta_{r'r} + t_x\,\delta_{r'r+e_x} + t_y\,\delta_{r'r+e_y} + h.c. \tag{6}$$

where $r = le_x + ne_y$ is a vector on the lattice with unit vectors $e_x = (1,0)$ and $e_y = (0,1)$. Furthermore, the nonzero matrix elements are given by:

$$\varepsilon_r = (m_{l,n} - 2\delta)\,\sigma_3, \quad t_x = \frac{1}{2}\,(\delta\sigma_3 - i\sigma_1), \quad t_y = \frac{1}{2}\,(\delta\sigma_3 - i\sigma_2).$$

Here it should be noticed that the invariance of the Hamiltonian (1) under the transformation $H \rightarrow -\sigma_1 H^* \sigma_1$ has been preserved under the discretization procedure.

For uniform gap m our new Hamiltonian reads in Fourier representation

$$\begin{aligned} H &= \sin(k_x)\sigma_1 - \sin(k_y)\sigma_2 + (m + \delta(\cos(k_x) \\ &\quad + \cos(k_y) - 2))\sigma_3 \\ &= h_1(k_x)\sigma_x - h_2(k_y)\sigma_2 + h_3(k_x, k_y)\sigma_3 \end{aligned} \tag{7}$$

with the dispersion

$$E = \pm\sqrt{h_1(k_x)^2 + h_2(k_y)^2 + h_3(k_x, k_y)^2}. \tag{8}$$

For $m = 0, \delta = 0$ there are four different nodes in the Brillouin Zone as it is indicated by the open circles in the left panel of Figure 1. We denote these points by Γ, Y, and X, where Y is two fold degenerate. For $m = 0$ and $\delta \neq 0$ there is a node at $(k_x, k_y) = (0,0)$ (Γ) and the nodes

at Y and X are gapped. For $m = 2\delta$ the nodes are located at Y or at X for $m = 4\delta$. The right panel of Figure 1 shows a plot of the dispersion equation (8). The node degeneracy can be lifted in this model via the parameter δ.

We absorb the index n with the help of matrix representation and write for the wave function

$$\psi_{l+1} = H^y \, \psi_l + H^D \, \psi_{l-1}. \qquad (9)$$

Each spinor component is now a M-component vector, where M is the width of a strip and thus $n = 1, 2, \ldots, M$. The matrices H^y, H^D read

$$H^y_{n,n} = t_x^{-1} \left[E \, \sigma_0 + (2\delta - m_n)\sigma_3 \right]$$

$$H^y_{n,n+1} = \frac{1}{2} t_x^{-1} \left[i\sigma_2 - \delta\sigma_3 \right]$$

$$H^y_{n,n-1} = -\frac{1}{2} t_x^{-1} \left[i\sigma_2 + \delta\sigma_3 \right]$$

$$H^D_{n,n} = -\frac{1}{2} t_x^{-1} \left[i\sigma_1 + \delta\sigma_3 \right]$$

where H^y contains periodic boundary conditions in the y-direction. This matrix structure allows us to construct a transfer matrix T_l through the equation [8]

$$\begin{pmatrix} \psi_{l+1} \\ \psi_l \end{pmatrix} = \begin{pmatrix} H^y & H^D \\ 1 & 0 \end{pmatrix} \begin{pmatrix} \psi_l \\ \psi_{l-1} \end{pmatrix} \equiv T_l \begin{pmatrix} \psi_l \\ \psi_{l-1} \end{pmatrix}. \qquad (10)$$

The introduction of a different random potential, e.g. random scalar potential, is straight forward.

Lyapunov exponents

According to [8,9] the transfer matrices T_l, defined in equation (10), can be used to calculate Lyapunov characteristic exponents (LCE). With initial values ψ_0 and ψ_1 the iteration of equation (10) provides ψ_L by the product matrix

$$M_L = \prod_{l=1}^{L} T_l. \qquad (11)$$

For disordered systems this is a product of random matrices that satisfies Oseledec's theorem [26]. The latter states that there exists a limiting matrix

$$\Gamma = \lim_{L \to \infty} \left(M_L^\dagger M_L \right)^{1/2L}. \qquad (12)$$

The eigenvalues of Γ are usually written as exponential functions $\exp(\gamma_i)$, where γ_i is the LCE. Adapting the numerical algorithm described in reference [8], the whole Lyapunov spectrum can be calculated and the smallest LCE is identified with the inverse localization length [9].

3 Numerical results for random gap

After introducing the model and the corresponding transfer matrices we calculate the inverse of the smallest LCE

$\Lambda = 1/\gamma_{min}$ which is identified as the localization length. Λ increases with the system width M according to a power law:

$$\Lambda \propto M^\alpha, \qquad (13)$$

where $\alpha > 1$ ($\alpha < 1$) in the regime of extended (localized) states, and $\alpha = 1$ in the critical regime. For the exponentially localized regime we expect $\Lambda \propto const$. According to the one-parameter scaling theory by MacKinnon and Kramer [27], the normalized localization length $\tilde{\Lambda} = \Lambda/M$ obeys the equation

$$\frac{d \ln \tilde{\Lambda}}{d \ln M} = \chi(\ln \tilde{\Lambda}), \qquad (14)$$

where χ is an unknown function with solutions of the form

$$\tilde{\Lambda}(M, W) = f(\xi(W)/M). \qquad (15)$$

The parameter W characterizes the disorder strength and ξ is a characteristic length of the system. The one-parameter scaling theory states that $\tilde{\Lambda}$ is not depending on M and W separately. Any change of disorder strength W can be compensated by a change of the system width M. Furthermore, from the behavior of $\tilde{\Lambda}$ in the vicinity of a scale-invariant point it is possible to calculate the critical exponent ν of the correlation length [8], which is the localization length of the infinite system. This is done by Taylor expansion

$$\ln \tilde{\Lambda} = \ln \tilde{\Lambda}_c + \sum_{s=1}^{S} A_s \left(|W - W_c| M^{1/\nu} \right)^s$$

$$= \ln \tilde{\Lambda}_c + \sum_{s=1}^{S} A_s \left(\frac{\xi}{M} \right)^{-s/\nu}, \qquad (16)$$

with $\xi = |W - W_c|^{-\nu}$. Comparing the latter with equation (15), the scaling function ξ can be interpreted as the characteristic length scale. We also have used the scaling ansatz of reference [14] but this did not provide a good fit to our data. On the other hand, the scaling behavior in this type of numerical analysis is limited by the finite width of the system. This means that we cannot rule out that there are corrections to the asymptotic behavior of the infinite system.

3.1 Preserved node symmetry: $\delta = 0$

In this case we have a four-fold degeneracy of the node structure. First we calculate Λ from transfer matrix (10) with $\delta = 0$. If it is not mentioned explicitly we use for the random gap m a box distribution on the interval $[\bar{m} - W/2, \bar{m} + W/2]$, where the corresponding variance is given by $W^2/12$. Furthermore, we restrict our calculations to the Dirac point (i.e. $E = 0$).

Figure 2 depicts the effect of the average gap $\bar{m}$ on the localization length Λ. The localization length always increases with system width M, indicating that there is no exponential localization. Only for very weak disorder
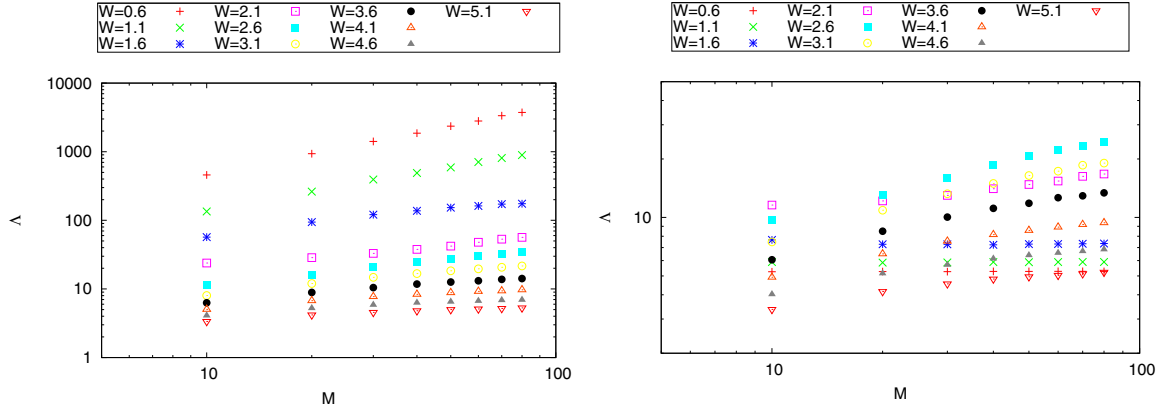
Fig. 2. Localization length for preserved node degeneracy ($\delta = 0$) with average gap $\bar{m} = 0$ (left panel) and $\bar{m} = 0.2$ (right panel) as a function of strip width M.
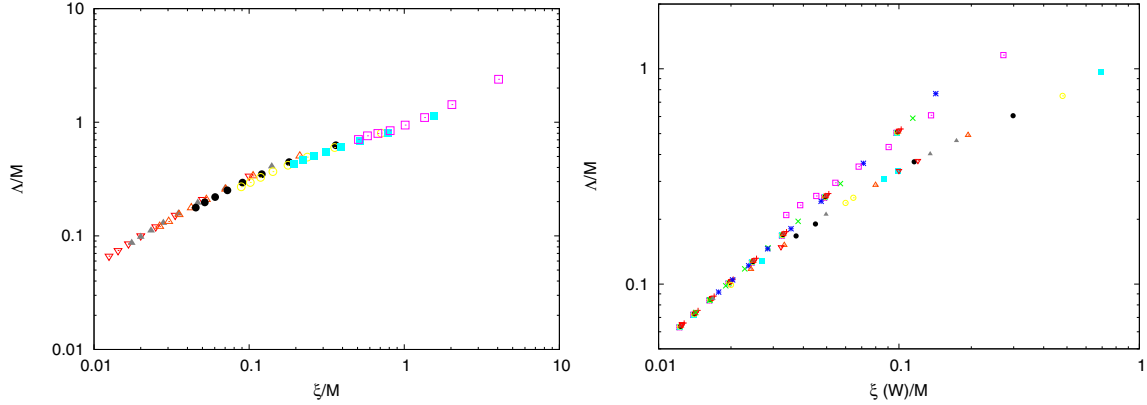

Fig. 3. Scaling plot of the localization length for $\delta = 0$, $\bar{m} = 0$ (left) and $\delta = 0$, $\bar{m} = 0.2$ (right). Left: rescaled without data for $W = 0.6; 1.1; 1.6$.

($W < 0.2$) and $\bar{m} = 0.2$ the localization length Λ is almost independent of M, which indicates exponential localization for $\bar{m} = 0.2$ (cf. Fig. 4a). As disorder increases the localization length decreases monotonically for $\bar{m} = 0$ but not for $\bar{m} = 0.2$ (cf. Fig. 2b). If we normalize Λ by strip width M and perform single parameter scaling as described in reference [8], almost all data points collapse to a single curve (cf. Fig. 3a). However, we had to neglect data points from weak disorder ($W \leq 1.6$) to see clearly a scaling behavior.

The behavior of Λ for a nonzero average gap ($\bar{m} = 0.2$) is more complex, as shown in Figures 3b and 4a. For weak disorder the localization length converges to a constant value for increasing M. As disorder increases Λ increases also but remains constant for large M. Then there is a transition at $W \approx 2.1$ where Λ is again growing with system size but the slope decreases with increasing disorder.

Due to this behavior of Λ as a function of disorder it is not possible to perform single parameter scaling in the common way. One approach to calculate the scaling function is to minimize the variance of $\ln M - \ln \xi$ for each localization length [27]. In a double logarithmic plot of $\tilde{\Lambda}$ the problem of one-parameter scaling translates then into shifting all curves onto one [8]. Since the position of

the resulting curve is irrelevant it is convenient to shift all curves onto the lowest i.e. that for biggest disorder. If one looks closely at the data in Figure 2 one sees that this is not possible only by shifting. Comparing to Figure 4 one can distinguish two regimes separated at $W \approx 2.1$. In both regimes one parameter scaling can be performed separately which gives two scaling functions for the infinite system. Additionally it is very important to point out that $\tilde{\Lambda}$ is always decaying with system size. Usually this is interpreted as localizing behavior. Whereas our analysis shows a rather unusual phase transition, namely that the correlation length diverges only when approaching the critical point from below W_c. In order to extract the functional behavior of ξ at the transition point we have fitted the data to several functions and found best agreement with

$$\xi(W) \propto |W - W_c|^{-\nu_L} \quad \text{for } 0 < W < W_c. \quad (17)$$

The results for the critical parameters are

$$\nu \approx 0.289 \pm 0.013 \quad (W_c \approx 2.156 \pm 0.009).$$

If we compare the variance g of the fitted critical disorder strength which is $g_c = 0.387$ to the gap width $2\bar{m} = 0.4$ we see a good agreement. A possible explanation for this might be that if fluctuations of the random gap are larger
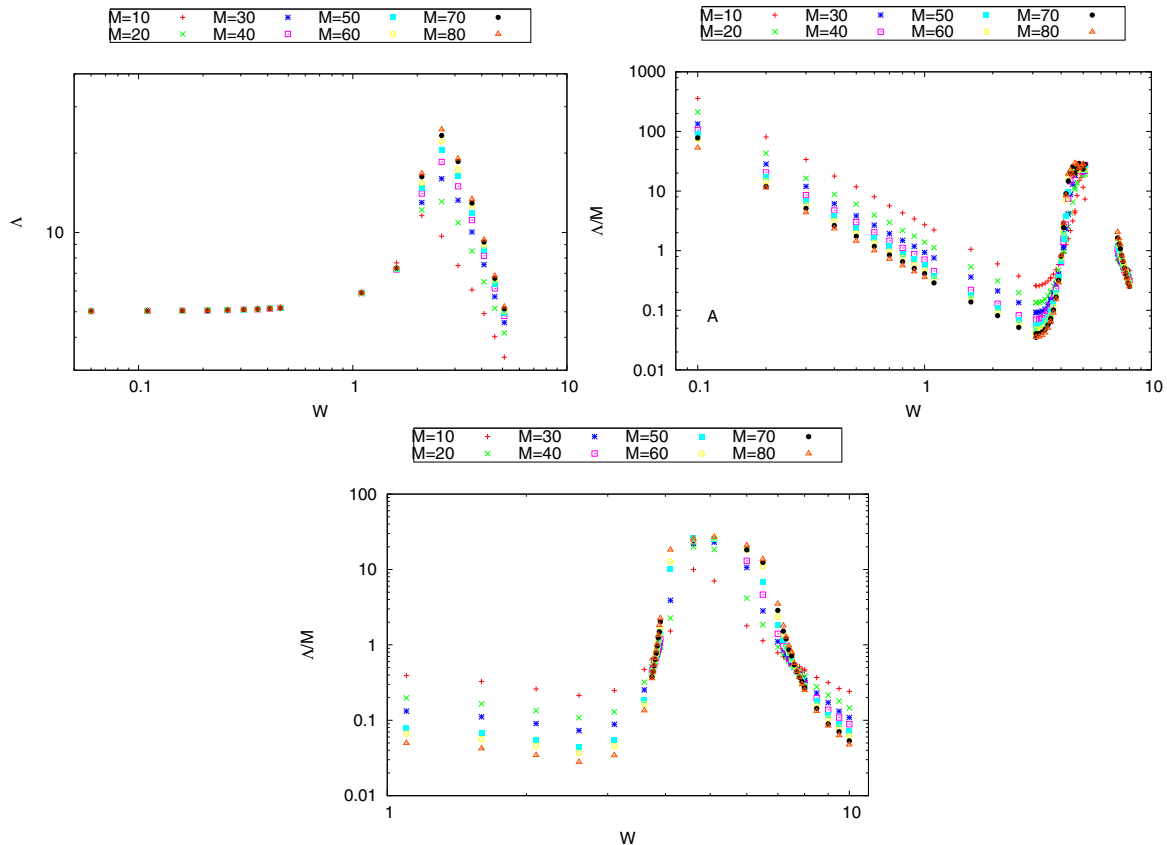
Fig. 4. Localization length for random gap with zero mean and broken node symmetry with ($\delta = 0.0$, $\bar{m} = 0.2$) (left), $\delta = 0.5$ and $\bar{m} = 0$ (right) and $\delta = 0.5$ and $\bar{m} = 0.2$ (bottom) as a function of disorder.

than the gap width states are no more exponentially localized and diffusive transport is possible. From this point of view we can also calculate W_c from the average gap width which yields $\tilde{W}_c \approx 2.191$. Fitting (17) with fixed critical disorder gives slightly different exponents but also a very good agreement with the numerical scaling function for $0 < W < W_c$:

$$\nu \approx 0.332 \pm 0.004 \quad (W_c \approx 2.191).$$

3.2 Broken node symmetry: $\delta \neq 0$

By setting $\delta = 0.5$ we break the four-fold degeneracy of the node structure and retain only the node at $k_x = k_y = 0$. Unlike in the case of $\delta = 0$ the localization length is not growing with system size if $\bar{m} = 0$. Figure 5a shows that for weak disorder Λ is constant with increasing M but decreases with increasing disorder W. However, for $W \geq 4.1$ Λ it increases with M (Fig. 5a). The normalized data is shown in Figure 4b. To keep the plot illustrative only a choice of the whole data is shown. What can be seen in Figure 4a is that for weak disorder up to $W = 3.6$ the normalized localization length decays for growing system sizes and scales to zero with M. For disorder larger than $W = 3.6$ $\tilde{\Lambda}$ is growing with system size. The growing localization length may be explained by comparison to the clean case. If fluctuations of the random gap are in

the range of 2δ a massless fermion appears. Thus disorder effectively closes the gap at the border of the Brillouin zone and the model shows metallic behavior.

For weak (i.e. $W \lessapprox 4$) and strong disorder (i.e. $W \gtrapprox 7.5$) the behavior is qualitatively the same, characterized by a decaying behavior of $\tilde{\Lambda}$ with increasing M. The benefit of plotting $\tilde{\Lambda}$ over W is that one can see directly two scale invariant points where different $\tilde{\Lambda}$ are intersecting for all available values of M. These points are indicative of phase transitions. Now we use the fitting functions of equation (16) to extract the critical exponent ν from our numerical result. For this purpose we set $s = 5$ and obtain the resulting curves in Figure 6. The critical parameters are listed in Table 1.

Using the scaling form of equation (15) all the curves collapse on two curves for a proper choice of the scaling function ξ, as depicted in Figures 7, 8. There plots agree qualitatively well for $\bar{m} = 0$, $\bar{m} = 0.2$, $\bar{m} = 0.8$ and $\bar{m} = -0.5$, the critical exponents for the second transition differ slightly though (cf. Tabs. 1–4).

3.2.1 Insulator-insulator transition

The reason that the model is not critical for $\bar{m} = 0$ is that it is not symmetric when replacing $m \rightarrow -m$. Instead it is symmetric around $\bar{m} = 1$. Nevertheless we expect a
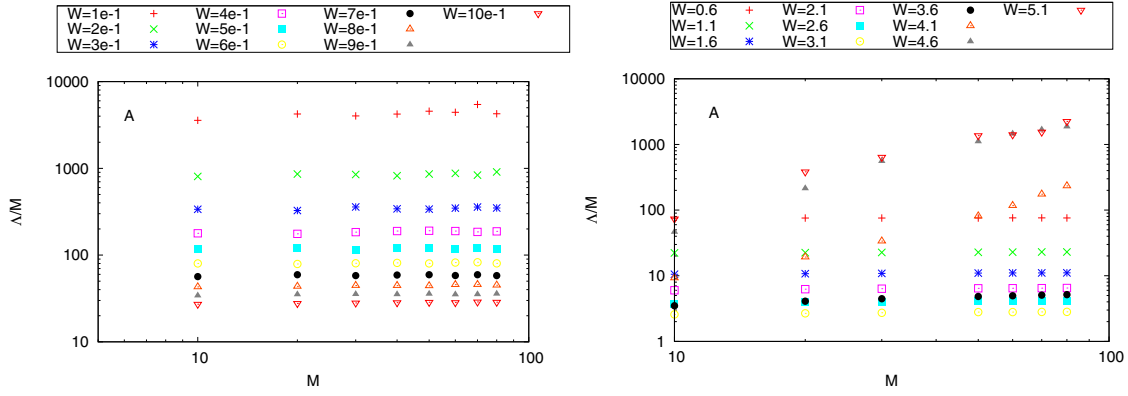
Fig. 5. Localization length for systems with zero average gap $\bar{m} = 0$ and broken node symmetry $\delta = 0.5$. Left and right panel are for different disorder ranges.
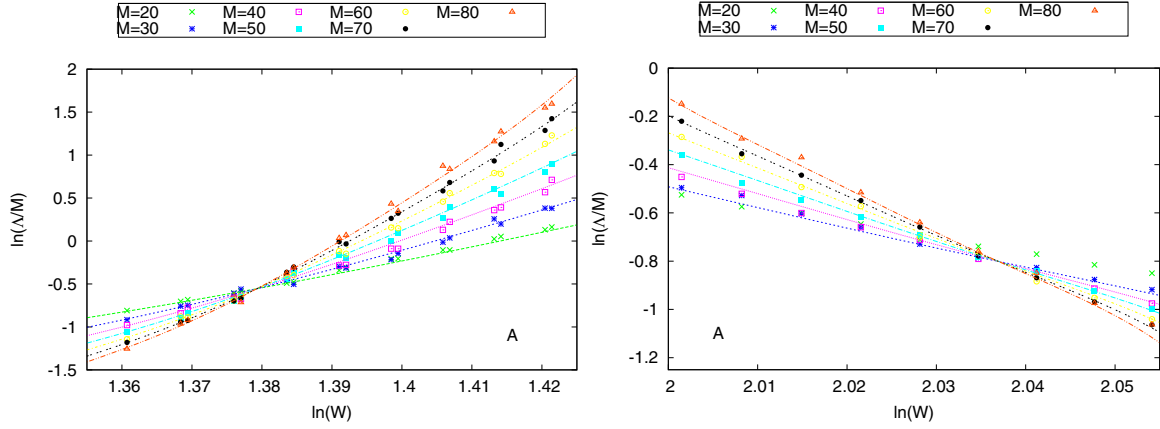

Fig. 6. Fits to equation (16) for $\bar{m} = 0$ and $\delta = 0.5$ around the critical point I (left) and around the critical point II (right).

Table 1. Critical values for $\bar{m} = 0$ and $\delta = 0.5$ obtained from fitting the data to equation (16).

Critical point	I	II
Exponent ν	1.297 ± 0.031	1.299 ± 0.066
W_c	3.975 ± 0.002	7.668 ± 0.008
Λ_c	0.574 ± 0.009	0.447 ± 0.005
Disorder range	$3.87 \leq W \leq 4.17$	$7.35 \leq W \leq 7.8$
System sizes	$20 \leq M \leq 80$	$30 \leq M \leq 80$

phase boundary separating two distinct insulating phases in vicinity of $\bar{m} \sim 0$, 2δ, 4δ where the localization length is independent of system size for disorder strengths smaller than W_{c1}. This means, that if we change $\bar{m}$ for fixed disorder, the system should undergo an insulator-insulator transition. Due to the asymmetry in m the phase boundary, at $\bar{m} \sim 0$, is shifted to negative $\bar{m}$ for increasing W. In order to confirm this assumption, we fix disorder strength and calculate Λ for different strip widths M as a function of $\bar{m}$. Discussing the inverse of the normalized localization length $z = M\gamma_{min}$ (or normalized Lyapunov exponent) is equivalent to discussing Λ/M [10] and numerical results are shown in Figure 9. Indeed, it can be seen that there

is a critical point at $\bar{m} < 0$. The critical exponent can be obtained by fitting the data to:

$$z = \frac{M}{\Lambda} \approx z_c + c \, (\bar{m} - m_c) M^{1/\nu}. \tag{18}$$

This has been done for three points in the $(\bar{m}, W)$-plane and the results for the critical exponents can be taken from Table 5.

3.2.2 Phase diagram

As described in the latter we have verified several critical points using finite-size scaling, where metal-insulator and insulator-insulator transitions occur. As a consequence, our analysis for the introduced model with broken node symmetry leads to a phase diagram shown in Figure 10. Since the model is symmetric around $\bar{m} = 2\delta$ only one half of the $(\bar{m}, W)$-plane is shown.

3.2.3 Suppression of the metallic regime

The metallic regime we have found is only present for a fluctuating mass with broken node symmetry. If we change
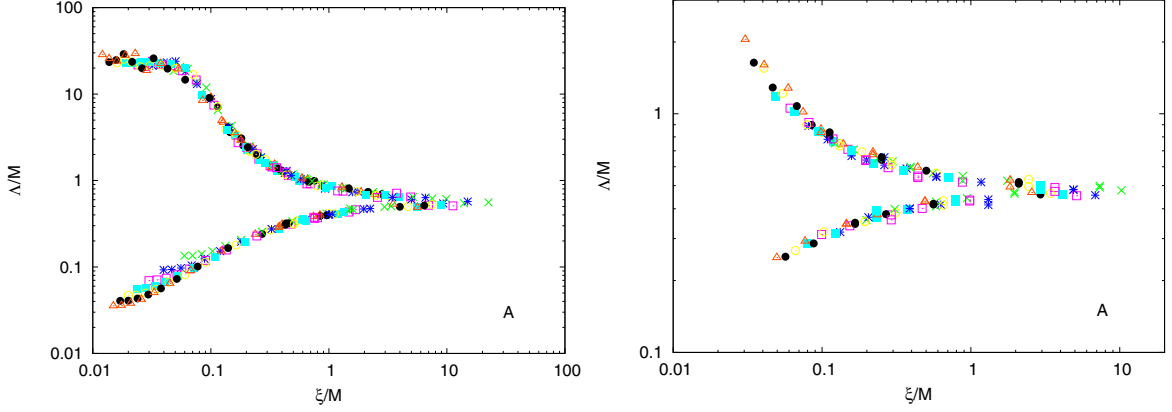
Fig. 7. Rescaled NLL for $\bar{m} = 0$ and $\delta = 0.5$ around the critical point I (left) and around the critical point II (right). Plots contain more data points than used for the fitting procedure to show the validity of one parameter scaling.
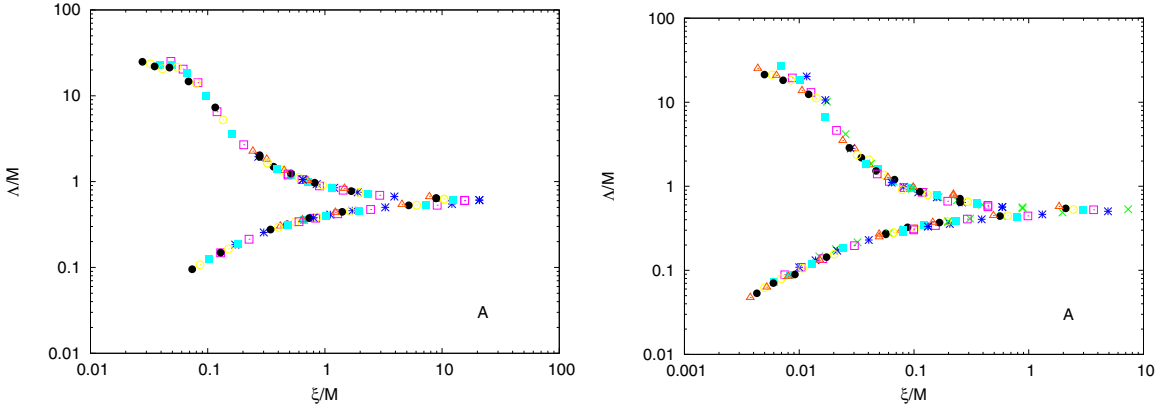

Fig. 8. Rescaled NLL for $\bar{m} = 0.2$ and $\delta = 0.5$ in the vicinity of critical point I (left) and in the vicinity of critical point II (right).

Table 2. Critical values for $\bar{m} = 0.2$ and $\delta = 0.5$ obtained from fitting the data to equation (16).

Critical point	I	II
Exponent ν	1.297 ± 0.045	1.397 ± 0.069
W_c	3.792 ± 0.002	7.629 ± 0.015
Λ_c	0.591 ± 0.007	0.517 ± 0.009
Disorder range	$3.72 \leq W \leq 3.88$	$7.1 \leq W \leq 8.0$
System sizes	$20 \leq M \leq 80$	$20 \leq M \leq 80$

Table 3. Critical values for $\bar{m} = 0.8$ and $\delta = 0.5$ obtained from fitting the data to equation (16).

Critical point	I	II
Exponent ν	1.217 ± 0.017	1.451 ± 0.024
W_c	3.047 ± 0.004	7.727 ± 0.01
Λ_c	0.893 ± 0.013	0.479 ± 0.007
Disorder range	$2.7 \leq W \leq 3.33$	$6.6 \leq W \leq 8.4$
System sizes	$20 \leq M \leq 80$	$20 \leq M \leq 80$

Table 4. Critical values for $\bar{m} = -0.5$ and $\delta = 0.5$ obtained from fitting the data to equation (16).

Critical point	I
Exponent ν	1.503 ± 0.026
W_c	4.379 ± 0.006
Λ_c	0.687 ± 0.010
Disorder range	$4.0 \leq W \leq 4.9$
System sizes	$20 \leq M \leq 80$

the type of disorder, for example from a scalar random potential to random gap, the behavior changes from insulating to metallic. For this purpose we introduce p which allows to tune the type of disorder as:

$$(1 - p)U_{l,n}\,\sigma_0 + p\,m_{l,n}\,\sigma_3, \qquad (19)$$

where we have chosen two independent random number distributions for $U_{l,n}$ and $m_{l,n}$ with same width W. In our numerical calculations we fix disorder strength to $W = 6$, where we expect metallic behavior in the case of random gap and tune p from scalar ($p = 0$) to random gap ($p = 1$). Moreover, numerical calculations show that the metallic behavior is already suppressed for values slightly below $p = 1$ (cf. inset in Fig. 11). A metallic phase for a different type of disorder can be found in the presence of spin-orbit coupling [28,29].
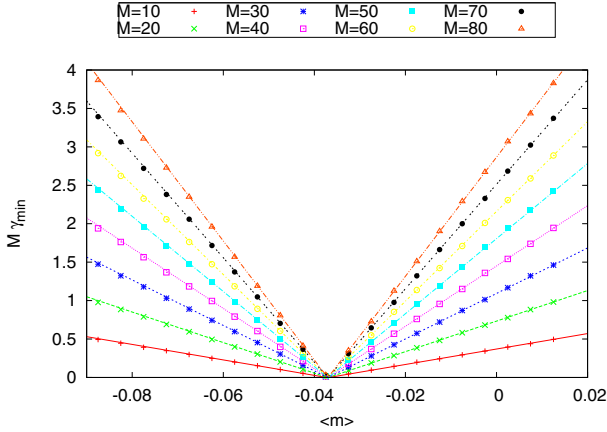
Fig. 9. Normalized Lyapunov exponent at the insulator-insulator transition for $\delta = 0.5$ and $W = 1$. Dashed lines correspond to the result of fitting equation (18) to the data.

Table 5. Critical exponents for the insulator-insulator transition.

Critical exponents		
$\nu = 1.019 \pm 0.001$	$(W = 1.0$	$m_c = -0.037)$
$\nu = 1.033 \pm 0.002$	$(W = 1.6$	$m_c = -0.095)$
$\nu = 1.006 \pm 0.005$	$(W = 1.0$	$m_c = 1.0)$

4 Discussion

Our numerical results can be summarized as follows. The localization length Λ always increases with M according to the power law of equation (13), where the exponent α depends on the model parameters:

$$\begin{cases} 0 < \alpha < 1 & \text{for } \delta = 0, \bar{m} = 0 \\ \alpha = 0 & \text{for } \delta = 0, \bar{m} = 0.2, W \leq W_c \\ 0 < \alpha < 1 & \text{for } \delta = 0, \bar{m} = 0.2, W > W_c \\ \alpha = 0 & \text{for } \delta = 0.5, \bar{m} = 0, 0.2, W \leq W_{c1} \\ \alpha > 1 & \text{for } \delta = 0.5, \bar{m} = 0, 0.2, W_{c1} \leq W \leq W_{c2} \\ \alpha = 1 & \text{for } \delta = 0.5, \bar{m} = m_c, W_{c1} \\ 0 < \alpha < 1 & \text{for } \delta = 0.5, \bar{m} = 0, 0.2, W > W_{c2} \end{cases}$$

(20)

where $\delta = 0$ represents the case with four degenerate nodes and $\delta = 0.5$ a single node. In our numerical results we can distinguish these to two cases: (I) for a preserved four-fold node degeneracy (i.e. $\delta = 0$) the gapless system has a monotonically increasing localization length with M as well as with W and does not indicate any transition. In the presence of a gap ($\bar{m} \neq 0$), however, there is a qualitative change at a characteristic disorder strength W_c: For $W < W_c$ the states are exponentially localized, whereas for $W > W_c$ they are not. It is not possible to decide within our numerical approach whether they are really extended or power-law localized in the gapped case. As discussed in Appendix, it might be sufficient for diffusion in a 2D system that the states obey a power law.

(II) For the single node (i.e. $\delta = 0.5$) the one-parameter scaling analysis of our results indicates a typical Anderson
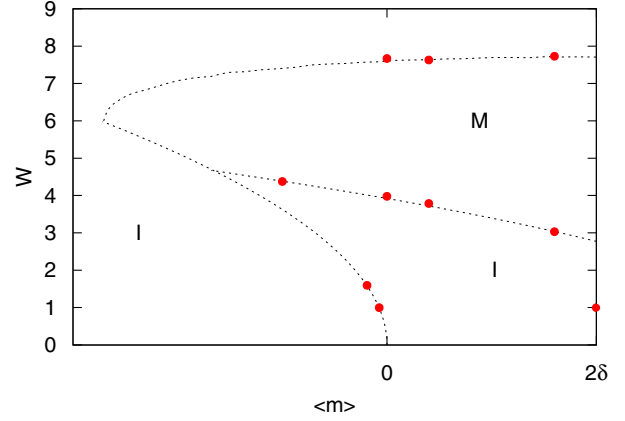

Fig. 10. Phase diagram for the case of broken node symmetry. Critical points (red points) have been obtained from finite-size scaling, broken lines are estimations of the phase boundaries.

transition at two critical points W_{c1}, W_{c2}. The exponent $\alpha = 0$ for weak disorder (i.e. for $W < W_{c1}$) indicates exponentially localized states. There is the intermediate metallic phase for $W_{c1} < W < W_{c2}$ with $\alpha > 1$ with one-parameter scaling behavior near the critical points. This is indicative of two metal-insulator transitions. In particular, there is a metal-insulator transition from $\alpha = 0$ to $\alpha > 1$ at a critical W_{c1}, which corresponds to a transition from $\alpha = 0$ to $0 < \alpha < 1$ for the gapped four degenerate Dirac nodes. The difference between a transition from $\alpha = 0$ to $0 < \alpha < 1$ and a transition from $\alpha = 0$ to $\alpha > 1$ is not clear from our numerical results. It could be that the latter is a genuine transition from exponentially localized to extended states, whereas the former is a transition from exponentially localized to power-law localized states. Furthermore, there are phase boundaries at $\bar{m} = m_c$ where the localization length shows critical behavior thus $\alpha = 1$.

5 Conclusion

We have introduced a model for Dirac fermions on a lattice with several nodes which allows us to perform numerical calculations of the localization length within the framework of the transfer matrix formalism. Using the Hamiltonian in equation (7) it is possible to break the node symmetry and to compare the properties for one and four nodal points in the Brillouin zone. We have shown that states in the gap can be localized and thus the localization length Λ converges to a finite value for increasing system size, whereas in the gapless case there are extended states as expected.

We have calculated the localization length for various system sizes and for different strength of the random gap. In all cases the localization length grows like a power law $\Lambda \sim M^\alpha$ with increasing system width M. However, the exponent α is quite sensitive to the model parameters (cf. (20)). In particular, this exponent vanishes for nonzero average gap and weak disorder, indicating exponential localization. Our numerical result also indicates $\alpha = 0$ for non-degenerate nodes, vanishing gap and weak disorder.
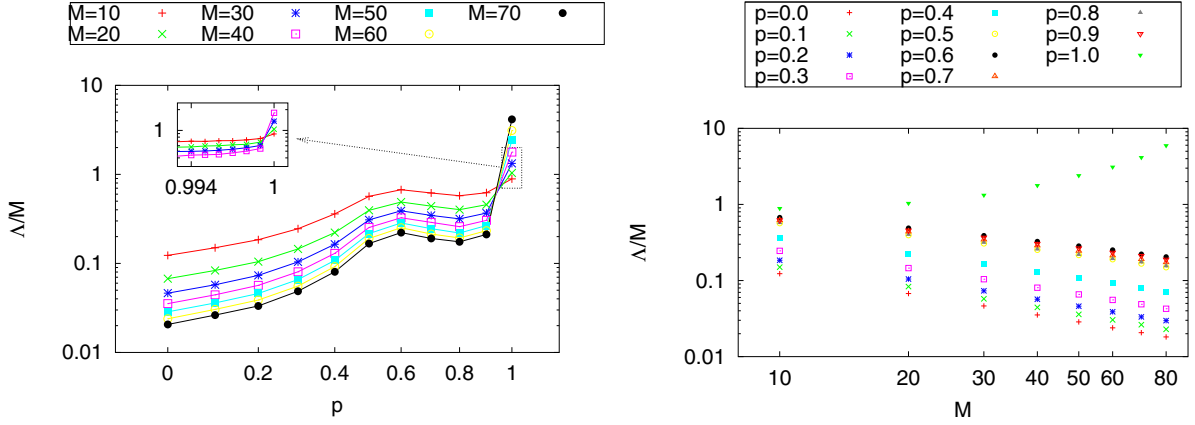
Fig. 11. NLL for $W = 6$, $\bar{m} = 0$ and $\delta = 0.5$ for the transition from random scalar potential to random gap. As a function of p (left) where the lines are guides for the eyes. The inset shows the behavior close to $p = 1$. The right panel shows the NLL as a function of system size.

On the other hand, we have $\alpha > 1$ only for intermediate disorder strength and non-degenerate nodes. Thus, the nodal degeneracy suppresses the intermediate phase. The latter is separated from the phases with $0 \leq \alpha < 1$ by transitions that obey one-parameter scaling behavior with scale-invariant critical points. This reflects the results of the weak-localization theory, where (anti-)localization has been found for (single) two nodes [4,6].

Our study was motivated by recent developments in the field of the 2D electron gas. Transport measurements on graphene, for instance, indicate that the effect of disorder on the electrons is rather weak. Our results confirm the robustness of the quantum states against Anderson localization if disorder is not too strong but it also indicates the possibility of an Anderson transition at sufficient strong disorder. Although the latter has not yet been observed in experiments, for instance, on graphene, it should be possible to find it on the surface of topological insulators, where disorder effects are stronger than in graphene. It might also be possible to create strong disorder in graphene by randomly removing carbon atoms with energetic particles [30]. The other important aspect is the tuning of the gaps as wells as the generation or removal of Dirac cones. Both are associated with an external symmetry breaking. This can be provided either by a periodic potential for the creation of new Dirac cones [31] or by structural doping with magnetic atoms [32].

Appendix: Localization and diffusion in 2D

Exponentially localized states rule out diffusive behavior. Here we briefly discuss that a power-law decaying state can provide diffusive behavior in a 2D electron gas. Diffusion of $|\Psi(\mathbf{r}, t)|^2$ in 2D is defined by the diffusion equation

$$\left(\frac{\partial}{\partial t} - \frac{D}{4} \nabla^2 \right) |\Psi(\mathbf{r}, t)|^2 = 0, \tag{A.1}$$

which has an expanding solution

$$|\Psi(\mathbf{r}, t)|^2 \equiv K(\mathbf{r}, \omega) \sim \frac{e^{-r^2/Dt}}{Dt} \quad (t \sim \infty).$$

The solution of equation (A.1) is also given by the diffusion propagator

$$\tilde{K}(q, \omega) = \frac{\bar{K}}{\omega + Dq^2}.$$

On the other hand, the localization length ξ in the spatial direction j can be defined as:

$$\xi = \sqrt{\sum_{\mathbf{r}} r_j^2 K(\mathbf{r}, \omega)},$$

where $K(\mathbf{r}, \omega)$ is connected with the diffusion propagator by a Fourier transformation:

$$K(\mathbf{r}, \omega) = \bar{K} \int \frac{e^{i\mathbf{q} \cdot \mathbf{r}}}{\omega + Dq^2} d^2q.$$

Using the Bessel function J_0 and the momentum cut-off λ for the q integral this result leads to:

$$K(\mathbf{r}, \omega = 0) - K(\mathbf{r}', \omega = 0) = \frac{\bar{K}}{D} \int_{\lambda r'}^{\lambda r} \frac{J_0(x)}{x} dx$$

and for $\lambda r', \lambda r \gg 1$

$$\sim \frac{\bar{K}}{D} \sqrt{\frac{2}{\pi}} \int_{\lambda r'}^{\lambda r} \frac{\cos(x - \pi/4)}{x^{3/2}} dx.$$

Thus $K(\mathbf{r}, \omega = 0)$ decays on large scales like $r^{-1/2}$. This reflects the fact that a decaying wave function leads to diffusion in 2D.

References

1. K.S. Novoselov, A.K. Geim, S.V. Morozov, D. Jiang, M.I. Katsnelson, I.V. Grigorieva, S.V. Dubonos, A.A. Firsov, Nature **438**, 197 (2005)
2. Y. Zhang, Y.-W. Tan, H.L. Stormer, P. Kim, Nature **438**, 201 (2005)
3. X.-L. Qi, S.-C. Zhang, Rev. Mod. Phys. **83**, 1057 (2011)
4. N.H. Shon, T. Ando, J. Phys. Soc. Jpn **67**, 2421 (1998)
5. J. Tworzydło, C.W. Groth, C.W.J. Beenakker, Phys. Rev. B **78**, 235438 (2008)
6. H. Suzuura, T. Ando, Phys. Rev. Lett. **89**, 266603 (2002)
7. Y.Y. Zhang, J. Hu, B.A. Bernevig, X.R. Wang, X.C. Xie, W.M. Liu, Phys. Rev. Lett. **102**, 106401 (2009)
8. A. MacKinnon, B. Kramer, Z. Phys. B **13**, 1546 (1983)
9. J.L. Pichard, G. Sarma, J. Phys. C **14**, L127 (1981)
10. P. Markoš, Acta Physica Slovaca **56**, 561 (2006)
11. J. Chalker, P. Coddington, J. Phys. C **21**, 2665 (1988)
12. K. Slevin, T. Ohtsuki, Phys. Rev. B **80**, 041304(R) (2009)
13. M. Schreiber, M. Ottomeier, J. Phys.: Condens. Matter **4**, 1959 (1992)
14. P. Markoš, L. Schweitzer, Phys Rev. B **81**, 205432 (2010)
15. A. Bostwick, J.L. McChesney, K.V. Emtsev, Th. Seyller, K. Horn, S.D. Kevan, E. Rotenberg, Phys. Rev. Lett. **103**, 056404 (2009)
16. D.C. Elias, R.R. Nair, T.M.G. Mohiuddin, S.V. Morozov, P. Blake, M.P. Halsall, A.C. Ferrari, D.W. Boukhvalov, M.I. Katsnelson, A.K. Geim, K.S. Novoselov, Science **323**, 610 (2009)
17. L.A. Ponomarenko, A.K. Geim, A.A. Zhukov, R. Jalil, S.V. Morozov, K.S. Novoselov, V.V. Cheianov, V.I. Fal'ko, K. Watanabe, T. Taniguchi, R.V. Gorbachev, Nat. Phys. **7**, 958 (2011)
18. D.S.L. Abergel, V. Apalkov, J. Berashevich, K. Ziegler, T. Chakraborty, Adv. Phys. **59**, 261 (2010)
19. K. Ziegler, Phys. Rev. Lett. **102**, 126802 (2009)
20. K. Ziegler, Phys. Rev. B **79**, 195424 (2009)
21. K. Nomura, N. Nagaosa, Phys. Rev. Lett. **106**, 166802 (2011)
22. L. Susskind, Phys. Rev. D **16**, 3031 (1977)
23. R. Stacey, Phys. Rev. D **26**, 468 (1982)
24. M.V. Medvedyeva, J. Tworzydło, C.W.J. Beenakker, Phys. Rev. B **81**, 214203 (2010)
25. K. Ziegler, Phys. Rev. B **53**, 9653 (1996)
26. V. Oseledec, Trans. Moscow Math. Soc. **19**, 197 (1968)
27. A. MacKinnon, B. Kramer, Phys. Rev. Lett. **47**, 21 (1981)
28. A. Yamakage, K. Nomura, K. Imura, Y. Kuramoto, J. Phys. Soc. Jpn **80**, 053703 (2011)
29. A. Yamakage, K. Nomura, K. Imura, Y. Kuramoto, Phys. Rev. B **87**, 205141 (2013)
30. L. Tapaszto, G. Dobrik, P. Nemes-Incze, G. Vertesy, P. Lambin, L.P. Biro, Phys. Rev. B **78**, 233407 (2008)
31. D.P. Arovas, L. Brey, H.A. Fertig, Eun-Ah Kim, K. Ziegler, New J. Phys. **12**, 123020 (2010)
32. A. Hill, A. Sinner, K. Ziegler, New J. Phys. **13**, 035023 (2011)